PCCP

Structure of intrazeolite molybdenum oxide clusters and their catalysis of the oxidation of ethyl alcohol

Yasuaki Okamoto,*[a] Nobuyuki Oshima,[a] Yasuhiro Kobayashi,[b] Osamu Terasaki,[c] Tetsuya Kodaira[d] and Takeshi Kubota[a]

[a] *Department of Material Science, Shimane University, Matsue, 690-8504, Japan.*
E-mail: yokamoto@riko.shimane-u.ac.jp
[b] *Department of Chemical Engineering, Osaka University, Toyonaka, 560-8531, Japan*
[c] *Department of Physics, Tohoku University, Sendai, 980-8578, Japan*
[d] *Nanoarchitectonics Research Center, National Institute of Advanced Industrial Science and Technology, Tsukuba, 305-8565, Japan*

Received 21st September 2001, Accepted 18th March 2002
First published as an Advance Article on the web 8th May 2002

Molybdenum oxide clusters confined in zeolite supercages were synthesized using a precursor $Mo(CO)_6$ adsorbed in the pores of zeolite and characterized by XAFS, HREM, LRS and XPS. The structure of the intrazeolite Mo oxide clusters and their catalysis of the oxidation of ethyl alcohol to acetaldehyde were investigated. It was found by Mo K-edge XAFS that intrazeolite Mo(VI) oxide dimer species with an octahedral symmetry of Mo are formed by thermal oxidation of $Mo(CO)_6$ entrapped in an NaY zeolite irrespective of the Mo loading up to two Mo atoms per supercage. HREM and XRD detected no degradation of the crystallinity of the host zeolite. The dimer catalyst showed a specific activity for the oxidation of ethyl alcohol 10 times higher than an impregnation catalyst, in which isolated tetrahedral Mo oxide species are formed. The Mo oxide dimer species were transformed to monomeric species by a heat treatment at 673 K. This led to a considerable decrease in catalytic activity. The Mo oxide clusters prepared by thermal oxidation of $Mo(CO)_6$ encaged in the cavity of a high silica FAU zeolite ($Si/Al = 630$) showed a significantly higher specific activity than the Mo oxide clusters in NaY. From the Mo K-edge EXAFS analysis, it was found that Mo oxide clusters containing several Mo atoms are constructed in the pores of the high silica zeolite. It is concluded that the structure and size of Mo oxide clusters encaged in zeolite are controlled by the zeolite composition and heat treatment and that larger Mo oxide clusters exhibit a higher specific activity for the partial oxidation of ethyl alcohol.

Introduction

Uniform and well-defined catalytically active species are anticipated to be formed when uniform supports and well-characterized metal precursors are utilized in the preparation of catalysts. Zeolites are widely appreciated as potential media for these purposes because of their uniform, homogeneous crystalline structures having unique, ordered pore systems on a molecular level.[1–5]

In the petrochemical industry, oxidation is by far one of the most important reactions and metal oxide catalysts have been used for selective oxidation reactions of alcohol and hydrocarbons. Molybdenum oxide based catalysts are widely used for these purposes.[6,7] It is well established that the catalysis of Mo oxides depends strongly on their surface structure.[8,9] It might be possible to control the structure of metal oxide clusters and, accordingly, their catalytic properties, by varying the zeolite structure and composition, when a transition metal complex encaged in zeolite is used to prepare the oxide clusters.

Many workers[10,11] have employed molybdenum hexacarbonyl $Mo(CO)_6$ encaged in cation exchanged zeolites to prepare Mo clusters with well-defined structure, such as Mo sulfide,[11–22] oxide,[23–26] oxy-carbide[27] and metal.[28] It was shown that the structure and size of the Mo sulfide clusters depend on the pore structure and composition of the host zeolite.[14,15,17] The preparation and structure of intrazeolite Mo oxide clusters have been studied by a variety of techniques including X-ray absorption fine structure (XAFS).[24–26] However, no catalytic properties of intrazeolite Mo oxide catalysts have been reported until now. It is of great interest to investigate the relation between the catalytic properties and the structure of Mo oxide clusters in zeolite. In the present study, we report the preparation of Mo oxide clusters in zeolite by thermal oxidation of $Mo(CO)_6$ encapsulated therein and the effect of the zeolite composition. The structure of the Mo oxide clusters is correlated to the catalytic activity for the oxidative dehydrogenation of ethyl alcohol to acetaldehyde as a test reaction.

Experimental

Catalyst preparation

NaY zeolite (JRC-Z-Y5.5, a reference catalyst provided by the Catalysis Society of Japan, $Si/Al = 2.8$) and a high silica FAU zeolite (HSi-FAU, Tosoh, $Si/Al = 630$), prepared by dealumination of NaY, were used as host zeolites. To synthesize zeolite supported Mo oxide catalysts, we employed two preparation methods; a chemical vapor deposition (CVD) method and a conventional impregnation method. In the CVD method, zeolite (0.1 g) was evacuated ($<10^{-3}$ Pa) at 673 K for 1.5 h and then exposed to $Mo(CO)_6$ vapor at room temperature for 16 h, unless otherwise noted, followed by evacuation for 10 min at room temperature to remove $Mo(CO)_6$ molecules physisorbed on the external surface of the zeolite. Thermal oxidation of $Mo(CO)_6$/zeolite was carried out at 353 K in the presence of 20 kPa of O_2 using a closed circulation system (volume : 0.20 dm^3). In order to ensure complete oxidation of $Mo(CO)_6$ to Mo(VI) oxides, the O_2 gas was evacuated and replaced every 3 h with 20 kPa of fresh O_2 until almost no formation of CO_2 and CO was detected (usually 3–4 times). The Mo oxide catalyst thus prepared is denoted CVD-MoO_3/zeolite. The Mo content was 10 wt.%, unless otherwise noted. The Mo content is shown by the number in parentheses, if necessary, as CVD-MoO_3/NaY (5) for CVD-MoO_3/NaY containing 5.3 wt.% Mo. CVD-MoO_3/NaY treated in vacuum at 673 K for 2 h is denoted CVD-MoO_3/NaY (ev). The Mo content was analyzed by X-ray fluorescence (XRF) (Rigaku, RIX-2000).

An NaY-supported Mo oxide catalyst (10 wt.% Mo) was also prepared by a conventional impregnation technique using an aqueous solution of $(NH_4)_6Mo_7O_{24}\cdot 4H_2O$. The catalyst was dried at 373 K and then calcined at 773 K for 3 h in an electric furnace. The Mo oxide catalyst thus prepared is denoted imp-MoO_3/NaY.

Catalytic reaction of ethyl alcohol oxidation

The catalytic oxidation of ethyl alcohol was carried out at 433 K using a closed circulation system. The initial partial pressures of C_2H_5OH and O_2 were 2.7 and 5.3 kPa, respectively. With CVD-MoO_3/zeolite, the reaction gas was introduced after evacuation at 433 K. With imp-MoO_3/NaY, the reaction was carried out after a pretreatment at 673 K for 1 h in the presence of 13.3 kPa of O_2, followed by evacuation and cooling to the reaction temperature, 433 K. The reaction gas was analyzed by an on-line gas chromatograph (TCD) using a column packing of Porapac PS (GL Science).

Catalyst characterization

XAFS measurement. Mo K-edge EXAFS and X-ray absorption near-edge structure (XANES) spectra for the Mo oxide/zeolite samples and reference compounds were measured in transmission mode at room temperature at BL-10B in the Photon Factory of Institute of Materials Structure Science, High Energy Accelerator Research Organization (KEK-IMSS-PF) with 2.5 GeV ring energy and 250–290 mA stored current. The synchrotron radiation was monochromatized by a Si (311) channel-cut monochromator. The intensities of incident and transmitted X-rays were counted by ion chambers with the applied voltages being 500 V. The XANES energy was calibrated by using the absorption edge of Mo metal at 20 003 eV. The energy resolution was 1.0 eV in the XANES region. The number of scans was three for each sample and the sum spectrum was used for further analysis.

The EXAFS data were analyzed using an analysis program developed by Technos (Osaka, Japan) and assuming a spherical wave approximation and a single scattering model. The analysis involves pre-edge extrapolation and background removal by a spline smoothing method to extract EXAFS oscillation. The EXAFS data were Fourier transformed from k-space (40–150 nm^{-1}) to R-space. The Fourier transforms were analyzed in R-space by a curve fitting procedure to obtain the coordination number N, bond distance R, Debye–Waller factor σ and inner potential E_0 using eqn. (2).

$$\chi(k_j) = S_jN_jF(k_j')\exp(-2k_j'^2\sigma_j^2)\sin(2k_j'R_j + \phi(k_j'))/k_j'R_j^2 \qquad (2)$$

where k_j' is the wave vector of a photoelectron and is expressed by eqn. (3).

$$k_j' = (k_j^2 - 2m\Delta E_{0j}/h^2)^{1/2} \qquad (3)$$

where m and ΔE_{0j} represent, respectively, the mass of an electron and the difference between the theoretical and experimental threshold energies. The empirical backscattering amplitude $F(k)$ and phase shift $\phi(k)$ for a Mo–Mo atomic pair were extracted from the EXAFS data for MoS_2 with R(Mo–Mo) = 0.316 nm and $N = 6$. The empirical parameters for an Mo–O bond were extracted from the EXAFS data for $Na_2MoO_4\cdot 2H_2O$ with R(Mo–O) = 0.1772 nm and $N = 4$. In both extractions of the empirical parameters, σ and E_0 were tentatively set at 0.006 nm and 0 eV respectively.

XPS and XRD measurements. The X-ray photoelectron (XP) spectra of the catalysts were measured on a Hitachi 507 (Al-$K\alpha_{1,2}$: 1486.6 eV). The sample was transferred to the pretreatment chamber using a N_2-filled glovebag. The binding energies were referenced to the Si 2p level from the host zeolite (NaY: 102.6 eV and dealuminated high silica FAU: 104.0 eV), which were separately determined for the corresponding untreated zeolites using the C 1s level at 285.0 eV due to adventitious carbon. The X-ray powder diffraction patterns of the catalyst samples were obtained on a RINT 2000 (Rigaku) after exposing to air just before the measurements.

LRS measurements. Fourier transform Raman spectra were obtained at room temperature on a Bruker RFS-100 instrument equipped with an FRA-106 sample stage. The power of the excitation light (1064 nm) from Nd-YAG laser was 10 mW for all measurements.

HREM observations. High-resolution electron microscopic (HREM) images of CVD-MoO_3/NaY and CVD-MoO_3/HSi-FAU were taken on a 400 kV EM, JEM-4000 EX, with a spherical aberration constant $C_s = 1.00$ mm, along the $\langle 100 \rangle$ direction. An NaY zeolite (Tosoh, Si/Al = 2.75), which had been confirmed by HREM to possess complete crystallinity even at the edge of the zeolite particles, was used for the preparation of CVD-MoO_3/NaY for HREM observations instead of JRC-Z-Y5.5. The sample was briefly exposed to air just before the HREM measurements.

Results

Catalytic oxidation of ethyl alcohol

The reaction products were exclusively acetaldehyde and diethyl ether. No reaction was observed to occur at 433 K over the host zeolite. The formation rate of acetaldehyde was significantly reduced when the reaction was carried out without gaseous O_2, indicating that acetaldehyde is catalytically produced by oxidative dehydrogenation of ethyl alcohol as observed for the oxidation of alcohol over Mo oxide catalysts.[29–37] On the other hand, the rate of diethyl ether formation was hardly affected by the presence of O_2, suggesting that diethyl ether is mainly produced by acidic sites.[38] Accordingly, we focus on the acetaldehyde formation as the oxidation activity of the Mo oxide catalyst hereafter.

The catalytic activities of the zeolite supported Mo oxides (10 wt.% Mo) are summarized in Table 1 for the oxidation of ethyl alcohol. It is evident that CVD-MoO_3/NaY shows an activity for the formation of the aldehyde 10 times higher than imp-MoO_3/NaY. However, when CVD-MoO_3/NaY was treated in a vacuum at 673 K for 2 h, the activity was decreased to 65% of the fresh catalyst. The reduced activity was not recovered by heat treatment at 673 K in the presence of gaseous O_2. It is remarkable that CVD-MoO_3/HSi-FAU exhibits an activity 16 times higher than the NaY-supported counterpart. All these results show that the activity of the Mo oxide/zeolite catalyst depends strongly on the zeolite used, the preparation method and the heat treatment.

In order to examine the effect of the Mo content on the activity, the Mo content in CVD-MoO_3/NaY was varied by

Table 1 Catalytic activities of Mo oxides supported on zeolite for the oxidation of ethyl alcohol at 433 K

Catalyst	Mo content (wt.%)	Rate of formation/μmol min^{-1} g^{-1}	
		Acetaldehyde	Diethyl ether
CVD-MoO_3/NaY	10	1.4	0.40
CVD-MoO_3/NaY (ev)	10	0.88	0.60
CVD-MoO_3/HSi-FAU	10	22	2.5
imp-MoO_3/NaY	10	0.12	0.10

changing the exposure time of degassed NaY to a vapor of $Mo(CO)_6$ at room temperature. Fig. 1 shows the Mo content as a function of the exposure time. After 12 h, the Mo content was saturated at 10 wt.% (2Mo/supercage) in line with the results of other workers.[10,15,24,27,28] When CVD-MoO_3/NaY (10) was exposed again to $Mo(CO)_6$ vapor for 16 h, the Mo content increased to 13 wt.% Mo. Fig. 2 shows the catalytic activity of CVD-MoO_3/NaY for the oxidation of ethyl alcohol against the Mo content. The activity to acetaldehyde formation increases proportionally as the Mo content increases to 10 wt.%, with an abrupt increase at 13 wt.%. On the other hand, the activity to diethyl ether formation increases linearly with increasing Mo content to 13 wt.%.

XPS characterization

CVD-MoO_3/NaY and CVD-MoO_3/HSi-FAU were white and slightly blue in color, respectively, after preparation. As shown in Fig. 3(b), the Mo $3d_{5/2}$ binding energy is 233.1 eV for CVD-MoO_3/NaY, indicating the formation of Mo(VI) oxide species in the fresh catalyst (MoO_3; 233.1 ± 0.2 eV). The absence of the peak at 228.5 eV due to $Mo(CO)_6$ (Fig. 3(a)) indicates a complete oxidation of the carbonyl species. The formation of Mo(VI) oxides was also confirmed for CVD-MoO_3/HSi-FAU (Mo $3d_{5/2}$: 232.9 eV, figure not shown). The slightly blue color of CVD-MoO_3/HSi-FAU (weak absorption bands at 865 and 690^{sh} nm) suggests the presence of a small fraction of Mo(V) species.[39] However, the present XPS measurements could not detect them within experimental accuracy. When CVD-MoO_3/NaY was evacuated at 673 K for 2 h, the sample changed from white to brown in color to form CVD-MoO_3/NaY

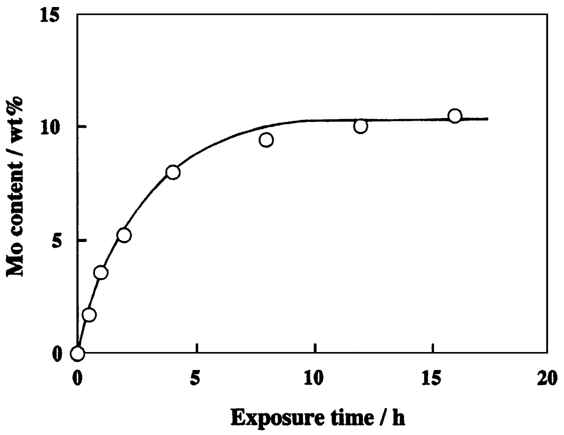

Fig. 1 Mo content in CVD-MoO_3/NaY as a function of the exposure time of NaY to a vapor of $Mo(CO)_6$ at room temperature.

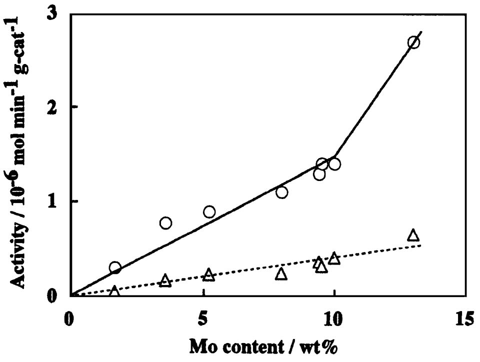

Fig. 2 Catalytic activity of CVD-MoO_3/NaY for the oxidation of ethyl alcohol at 433 K as a function of Mo content. (○) acetaldehyde and (△) diethyl ether.

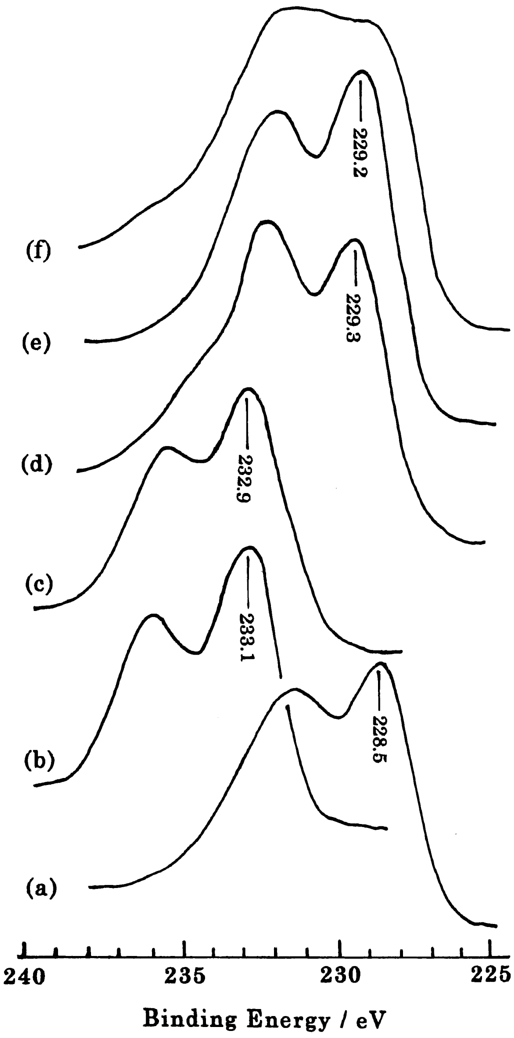

Fig. 3 X-Ray photoelectron spectra of the Mo 3d level for (a) $Mo(CO)_6$/NaY, (b) CVD-MoO_3/NaY (10), (c) CVD-MoO_3/NaY (ev), (d) CVD-MoO_3/NaY H_2-treated at 673 K for 2 h, (e) CVD-MoO_3/NaY H_2-treated at 873 K for 2 h and (f) imp-MoO_3/NaY H_2-treated at 873 K for 2 h.

(ev). As shown in Fig. 3(c), the XPS spectrum was only slightly broadened but no significant shift in the Mo $3d_{5/2}$ binding energy was observed (232.9 eV) on evacuation. Although the change in color suggests reduction of a part of the Mo(VI) to lower valence Mo species such as Mo(IV),[25] during the evacuation, the fraction of reduced Mo may be very small. On heat treatment of CVD-MoO_3/NaY at 673 K in the presence of O_2 (20 kPa), the sample remained white in color.

When CVD-MoO_3/NaY was treated at 673 K for 2 h in a stream of atmospheric pressure of H_2, the reduction of Mo(VI) species was apparently observed as depicted in Fig. 3(d). When CVD-MoO_3/NaY was H_2-treated at 873 K for 2 h (Fig. 3(e)), the weak hump around 234 eV observed in Fig. 3(d) disappears. It is most likely, on the basis of the spectral width, that the Mo species with the Mo $3d_{5/2}$ binding energy of 229.2 eV are predominantly formed after the H_2-treatment at 873 K. These species are assigned possibly to Mo(III) species on the basis of the published binding energies[40] (Mo(VI): 232.7 eV, Mo(IV): 229.6 eV, Mo(III): 228.8 eV, Mo(II): 228.2 eV). Fig. 3(f) also presents the reduction behaviour of imp-MoO_3/NaY at 873 K. It is obvious from an unresolved broad spectral feature that several kinds of Mo species are simultaneously formed in imp-MoO_3/NaY in contrast to the predominating Mo(III) species in CVD-MoO_3/NaY. The remarkably different reduction behaviour of the Mo oxide species in CVD- and imp-MoO_3/NaY indicates the formation of distinctly different Mo oxide species in these catalysts.

LRS characterization

Fig. 4 depicts the LRS spectra for CVD-MoO_3/NaY (a), CVD-MoO_3/HSi-FAU (b) and imp-MoO_3/NaY (c). The spectrum for MoO_3/SiO_2 (6.7 wt.% Mo) is also presented (d) to show the LRS spectrum characteristic of MoO_3 (995 and 818 cm^{-1}). The bands at 972 (NaY) and 997 cm^{-1} (HSi-FAU) are ascribed to Mo=O fundamental stretching vibrations. It is likely that the broad structures around 820–830 cm^{-1} are due to the stretching mode of Mo–O–Mo linkages.[41–43] In both LRS spectra for the CVD-catalysts, the formation of MoO_3 is entirely excluded by the absence of the sharp peaks due to MoO_3. With imp-MoO_3/NaY (Fig. 4(c)), a sharp band characteristic of MoO_4^{2-} interacting with a surface (Mo=O stretching band)[41–43] is observed at 938 cm^{-1}, indicating the formation of isolated Mo oxide species in tetrahedral configurations.

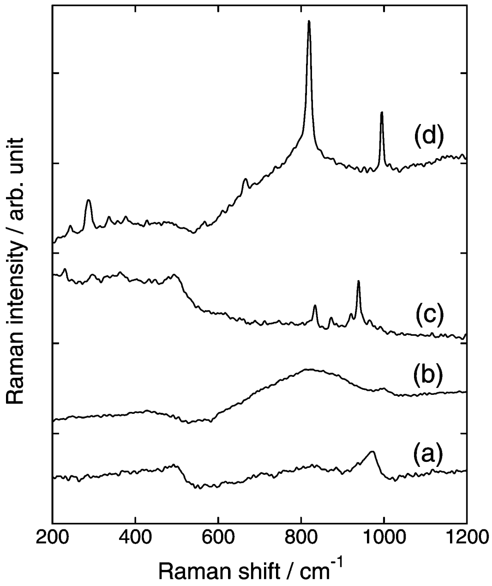

Fig. 4 FT-Raman spectra of (a) CVD-MoO_3/NaY, (b) CVD-MoO_3/HSi-FAU, (c) imp-MoO_3/NaY and (d) MoO_3/SiO_2.

XRD results

Fig. 5 compares the XRD patterns for CVD-MoO_3/NaY and imp-MoO_3/NaY with that for the host zeolite NaY. With CVD-MoO_3/NaY (a), neither an XRD peak ascribable to crystalline MoO_3 nor degradation of the crystal structure of the NaY are observed. Scrutinizing the XRD pattern (a) indicates that the relative intensities of a few diffraction peaks such as (111) and (220) are remarkably reduced by the accommodation of Mo oxides, strongly suggesting that Mo oxides are located inside the zeolite pores.[15] In the case of imp-MoO_3/NaY, however, the XRD pattern (b) shows a considerable degradation of the crystallinity of the host zeolite, in line with the observations of other workers.[44–47]

HREM observations

Fig. 6 presents the HREM image of CVD-MoO_3/NaY. Obviously, it is concluded that the crystal structure of the host zeolite is not destroyed at all by the accommodation of $Mo(CO)_6$ and successive oxidation at 353 K. In addition, no agglomerated Mo oxide species are observed on the external

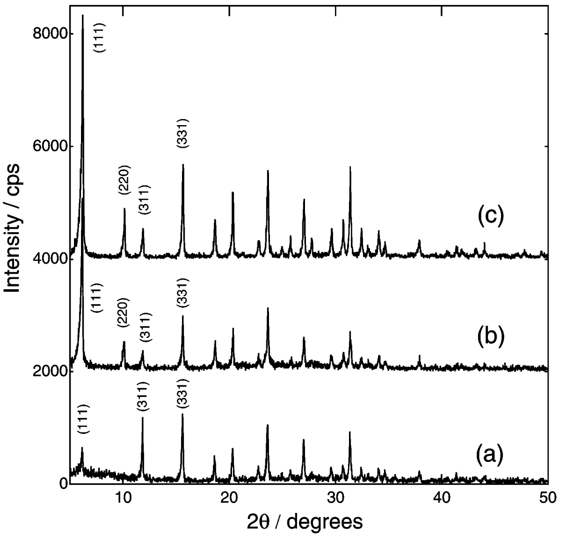

Fig. 5 XRD patterns of (a) CVD-MoO_3/NaY, (b) imp-MoO_3/NaY and (c) NaY.

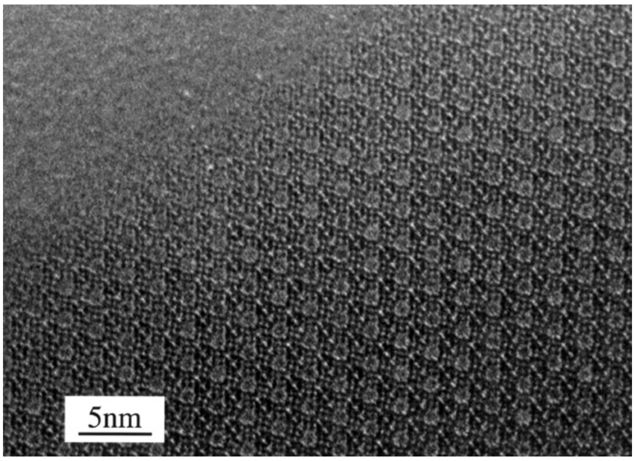

Fig. 6 An HREM image of CVD-MoO_3/NaY (10); 400 kV EM, [110] incidence.

surface of the host zeolite. Accordingly, it is inferred that the Mo oxide species are located inside the zeolite cages, as suggested by the XRD results. The HREM observations were consistent with the XRD results, showing no degradation of the crystallinity of the zeolite and no diffraction peaks due to MoO_3. The HREM observations for CVD-MoO_3/HSi-FAU (not shown) led to the same conclusions as for CVD-MoO_3/NaY.

XAFS characterization

The structure of Mo oxides prepared in the zeolite cavities was studied by means of EXAFS and XANES. Fig. 7 shows k^3-weighted Mo K-edge EXAFS oscillations for some representative catalyst systems; imp-MoO_3/NaY, CVD-MoO_3/NaY, CVD-MoO_3/NaY (ev) and CVD-MoO_3/HSi-FAU. The Fourier transforms for the catalysts and some reference compounds are presented in Fig. 8 and Fig. 9, respectively. From a comparison of the Fourier transforms for $Mo(CO)_6$/NaY and the CVD-catalysts, it is concluded that $Mo(CO)_6$ in the zeolite is completely converted to Mo oxide species, in agreement with the XPS results (Fig. 3(a) and (b)). Comparison of the Fourier transforms (Fig. 8(b)–(d)) for the MoO_3/zeolite catalysts derived from $Mo(CO)_6$ with that for MoO_3 (Fig. 9(a)) or Na_2MoO_4 (Fig. 9(b)) evidently indicates the formation of Mo oxide species having distinctly different structures from the reference compounds. On the other hand, the Fourier transform for imp-MoO_3/NaY (Fig. 8(a)) is close to that for Na_2MoO_4. The structural parameters of the zeolite-supported MoO_3 catalysts, as derived from the EXAFS analysis by using the empirical back-scattering amplitudes and phase shifts, are listed in Table 2. The representative curve-fitting results are shown in Fig. 10.

With the Fourier transform for CVD-MoO_3/NaY (10), the peak at 0.28 nm (phase shift: uncorrected) in Fig. 8(c) is assigned to a Mo–Mo second shell, indicating the formation of Mo oxide clusters in NaY zeolite cages rather than monomeric species. The Mo–O region was reasonably curve-fitted only by assuming two Mo–O bonds. The shorter Mo–O bond at 0.172 nm is ascribed to a Mo=O double bond, while the longer one at 0.193 nm to a Mo–O single bond. The coordination number (0.8) of Mo–Mo is close to unity, suggesting the formation of Mo_2O_6 dimer oxide clusters on the basis of the XPS results which indicate the formation of Mo(VI) oxides. With CVD-MoO_3/NaY (5), an essentially identical Fourier transform (Fig. 8(b)) and structural parameters are obtained (Table 2).

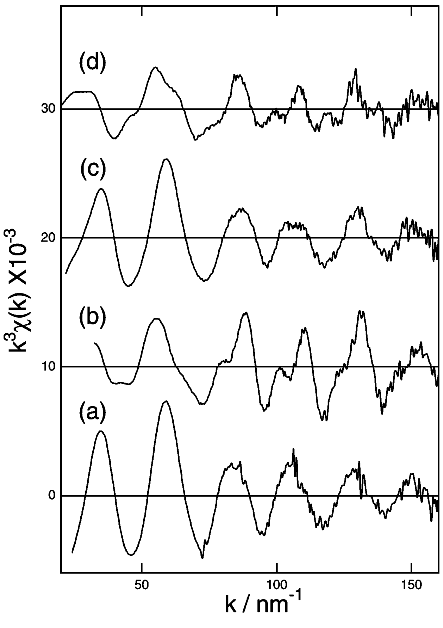

Fig. 7 Background-subtracted, k^3-weighted EXAFS functions of the Mo K-edge for (a) imp-MoO_3/NaY, (b) CVD-MoO_3/NaY, (c) CVD-MoO_3/NaY (ev) and (d) CVD-MoO_3/HSi-FAU.

Fig. 8(d) shows the k^3-weighted Fourier transform of Mo K-edge EXAFS for CVD-MoO_3/HSi-FAU. Two Fourier transform peaks are observed at 0.30 and 0.32 nm (phase shift: uncorrected) in the region of Mo–Mo. The structural parameters are also shown in Table 2. The parameters for Mo–Mo indicate that in CVD-MoO_3/HSi-FAU, Mo oxide species having a size larger than a dimer are constructed in the pores. With imp-MoO_3/NaY, the structural parameters are close to those for Na_2MoO_4. In conformity with the LRS results, the Mo oxide species in imp-MoO_3/NaY are assigned to monomeric Mo oxides in tetrahedral configurations.

Thermal stability of the Mo dimer species in CVD-MoO_3/NaY was examined by EXAFS. As shown in Fig. 11, the intensity of the Fourier transform peak at 0.28 nm due to Mo–Mo is significantly reduced after evacuation at 673 K (b), suggesting a degradation of the Mo oxide dimer species to monomeric species or to non-uniform Mo oxide clusters considerably disordered in the structure. Similarly, the Fourier transform peak at 0.28 nm was considerably decreased in intensity when CVD-MoO_3/NaY was heat treated at 673 K in the presence of gaseous O_2 (Fig. 11(c)). Accordingly, it is concluded that the structure of the dimer species is considerably unstable at 673 K even in the presence of gaseous O_2. When CVD-MoO_3/NaY was H_2-reduced at 873 K for 2 h (Fig. 11(d)), the Fourier transform changed greatly and a strong peak due to Mo–Mo appeared. The Mo–Mo atomic distance being larger than that for Mo metal and the presence of two kinds of Mo–O bonds indicate the formation of agglomerated, low valence Mo oxide species rather than a mixture of Mo oxides and Mo metal.

Fig. 12 shows the Mo K-edge XANES spectra for CVD-MoO_3/NaY, CVD-MoO_3/NaY (eV), CVD-MoO_3/HSi-FAU and imp-MoO_3/NaY. The Mo K-edge XANES spectra for Na_2MoO_4 and MoO_3 are also presented in Fig. 12 as reference compounds. It is well established that XANES spectra vary with the symmetry of the local structure of the X-ray absorbing atom (Mo).[48] A weak peak appearing in the pre-edge region (20 005–20 010 eV) is assigned to a 1s → 4d quadrupole transition. When Mo atoms have no inversion center, as in Na_2MoO_4, the 1s → 4d pre-edge peak intensity is enhanced by hybridization of the 4d states with p-type wave functions. Thus slightly distorted octahedral MoX_6 gives only a weak 1s → 4d pre-edge peak as observed for MoO_3, whereas a significantly distorted octahedral or tetrahedral MoX_n shows a stronger pre-edge peak as exemplified by Na_2MoO_4. A relative pre-edge peak intensity for the Mo oxides in Fig. 12 is summarized in Table 3, together with the peak position. The pre-edge peak energy for Na_2MoO_4 is slightly lower than that for MoO_3.

The first derivatives of the XANES spectra in Fig. 12 are compared in Fig. 13 to more clearly characterize the CVD-MoO_3/zeolite catalysts. The peak position around 20.00 keV corresponds to the edge energy and is summarized in Table 3. The edge energies for the MoO_3/zeolite catalysts are between those for Na_2MoO_4 and MoO_3. However, it is noteworthy from the spectral feature that the peak at about 20.00 keV for the catalyst consists of a single peak rather than a convoluted one of the peaks due to Na_2MoO_4 and MoO_3. This allows us to conclude that the Mo oxide species in the catalyst are composed of mainly specific Mo species rather than a mixture of MoO_3 clusters and MoO_4^{2-} species.

With imp-MoO_3/NaY, the intensity and position of the 1s → 4d pre-edge peak are very close to the values for Na_2MoO_4, indicating that the Mo species have tetrahedral symmetry. On the other hand, the intensity and position of the pre-edge peak for CVD-MoO_3/NaY are between those

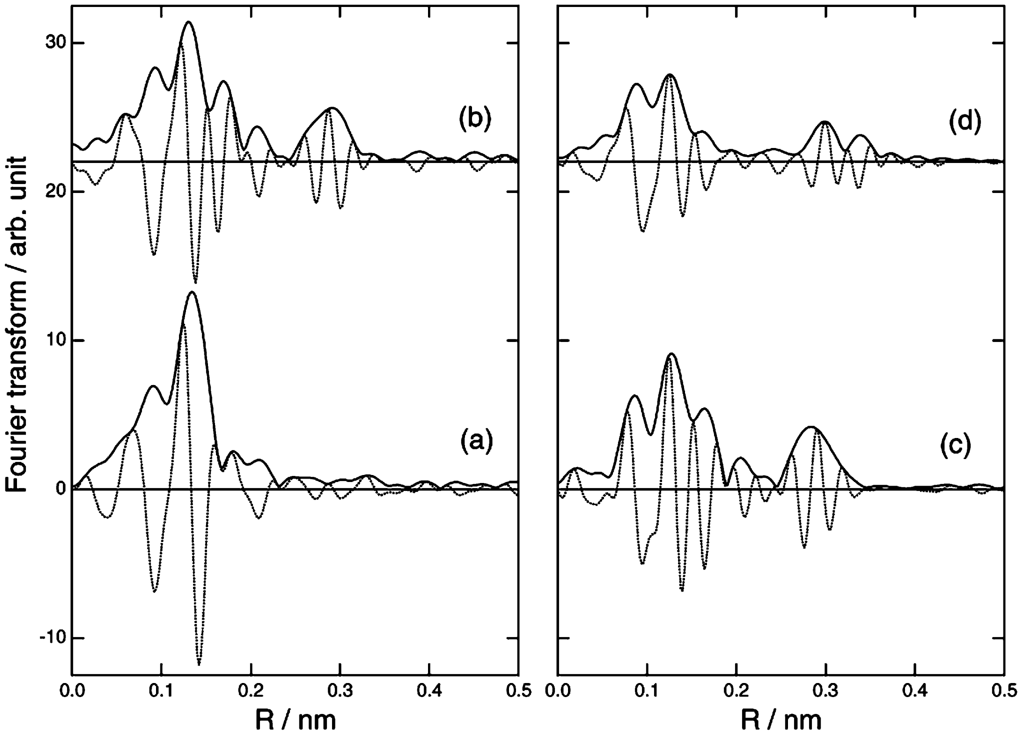

Fig. 8 Fourier transforms of k^3-weighted EXAFS modulations ($\Delta k = 40$–150 nm^{-1}) of the Mo K-edge for (a) imp-MoO_3/NaY, (b) CVD-MoO_3/NaY (5), (c) CVD-MoO_3/NaY (10) and (d) CVD-MoO_3/HSi-FAU.

for Na_2MoO_4 and MoO_3, indicating that the Mo species have a considerably distorted octahedral symmetry. The pre-edge peak intensity of CVD-MoO_3/NaY is slightly increased by the evacuation at 673 K. It is considered that the Mo species in CVD-MoO_3/NaY (ev) is still in a distorted octahedral symmetry, although the local structure is considerably altered. With CVD-MoO_3/HSi-FAU, a weak pre-edge peak evidently indicates that the local symmetry of the Mo atoms in the clusters is very close to that in MoO_3. In addition, the XANES spectrum for CVD-MoO_3/HSi-FAU (Fig. 12) shows three peaks, although much less resolved, at about 200 026, 200 038 and 200 052 eV characteristic of MoO_3, suggesting the formation of Mo oxide clusters having a local structure similar to that of MoO_3.

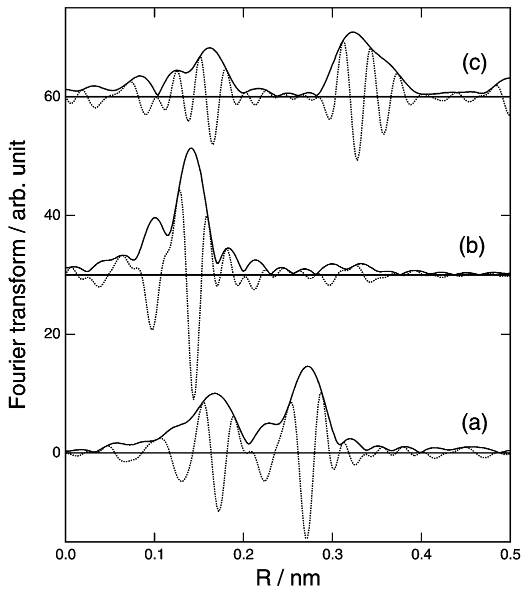

Fig. 9 Fourier transforms of k^3-weighted EXAFS oscillations ($\Delta k = 40$–150 nm^{-1}) of the Mo K-edge for reference compounds. (a) $Mo(CO)_6$/NaY, (b) $Na_2MoO_4 \cdot 2H_2O$ and (c) MoO_3.

Discussion

Location and structure of intrazeolite Mo oxide clusters

The location of the Mo oxide species, that is, inside or outside the zeolite pores, is of great importance to the control of the size and structure of the clusters and to the catalytic performance. The HREM image in Fig. 6 for CVD-MoO_3/NaY clearly demonstrates that the crystal structure of the host zeolite is not degraded by the incorporation of the Mo oxide clusters and that no agglomeration of Mo oxides takes place on the external surface of the zeolite. The LRS and XRD results support the HREM observations. In our previous study,[15] the pore volume of CVD-MoO_3/NaY was measured by using benzene as an adsorbate. The pore volume of CVD-MoO_3/NaY (10) was 0.169 cm^3 g^{-1} compared to 0.298 cm^3 g^{-1} for NaY. The decrease in the pore volume of 0.13 cm^3 g^{-1} is even greater than that expected from the volume of MoO_3 (*ca.* 0.06 cm^3 g^{-1}), indicating that Mo oxide species are formed inside the zeolite pores. It is concluded that, with CVD-MoO_3/NaY, the Mo oxide species are formed in the pores of NaY. It is inferred from the HREM observations that, with CVD-MoO_3/HSi-FAU, Mo oxide species are also formed in the supercage of the host zeolite. The location of the Mo oxide species in imp-MoO_3/NaY is not clear in the present study. However, taking into consideration the predominant formation of tetrahedral Mo oxide interaction species and a low external surface area of zeolite, it is likely that most of the Mo oxide species migrate into the pores of the host zeolite, with considerable destruction of the zeolite structure.

On the basis of the XPS results, it is concluded that the chemical state of the Mo atoms in the freshly prepared CVD-MoO_3/NaY is Mo(VI) oxide species. The $Mo(CO)_6$ molecules encapsulated in the NaY zeolite pores thermally decompose at 330–400 K to form subcarbonyl species, $Mo(CO)_x$ ($x = 5$,

Table 2 Structural parameters[a] as derived from the Mo K-edge EXAFS for molybdenum oxides encaged in zeolites

Catalyst	Treatment	Atom pair	R/nm	CN	E_0/eV	$\Delta\sigma^2/10^{-6}$ nm^2
CVD-MoO_3/NaY (10)	Fresh	Mo–O	0.172	2.9	−10.3	12
		Mo–O	0.193	2.3	−11.2	12
		Mo–Mo	0.322	0.8	−6.6	−6
	Evac. at 673 K	Mo–O	0.171	3.7	−9.1	41
	O_2-treat. at 673 K	Mo–O	0.170	4.2	−13.6	40
	H_2-treat. at 873 K	Mo–O	0.165	1.2	9.3	58
		Mo–O	0.208	2.8	−5.7	40
		Mo–Mo	0.278	3.2	−0.9	33
CVD-MoO_3/NaY (5)	Fresh	Mo–O	0.170	3.4	−7.5	26
		Mo–O	0.194	1.9	−2.7	16
		Mo–Mo	0.321	0.7	0.6	−6
CVD-MoO_3/HSi-FAU	Fresh	Mo–O	0.176	2.8	−13.4	38
		Mo–O	0.193	2.7	−13.9	74
		Mo–Mo	0.334	1.6	−0.3	47
		Mo–Mo	0.358	0.8	8.7	17
imp-MoO_3/NaY	Fresh	Mo–O	0.172	4.5	−10.9	17
$Mo(CO)_6$/NaY	Fresh	Mo–C	0.207	6.3	0.1	6
		Mo–C$\underline{O}$	0.322	5.7	0.1	0
Reference compound						
MoS_2		Mo–Mo	0.316	6		
$Na_2MoO_4 \cdot 2H_2O$		Mo–O	0.177	4		
Mo metal		Mo–Mo	0.2726	8		
			0.3147	6		

[a] R: bond distance, CN: coordination number, E_0: inner potential, σ: Debye–Waller factor.

4, 3).[10,49–53] In the present preparations at 353 K, the resultant subcarbonyl species readily react with gaseous O_2 to form Mo oxide species. In the case of photooxidation of $Mo(CO)_6$/NaY at room temperature, $Mo(CO)_6$ is decarbonylated by UV-irradiation to subcarbonyl species, which subsequently react with gaseous O_2 to form Mo(VI) oxide species (Mo $3d_{5/2}$: 233.0 eV).[26] According to Almond *et al.*,[54,55] W subcarbonyl species react with O_2 molecules to form monomeric W(VI) oxide species in a liquid Ar matrix (10 K). It is deduced that the formation of the subcarbonyl species and subsequent oxidation under moderate conditions are the most important processes to synthesize intrazeolite Mo oxide species.

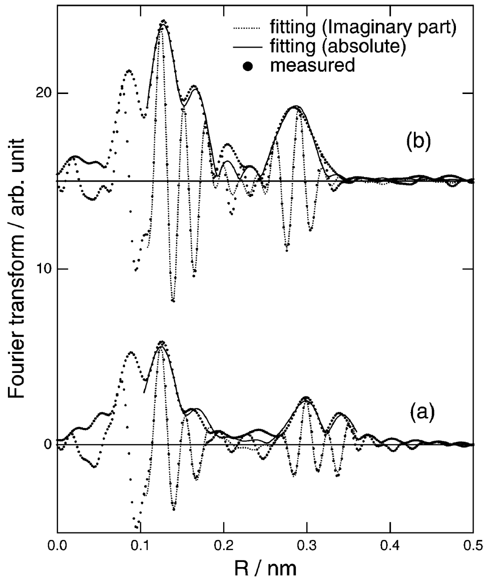

Fig. 10 Fourier transforms of k^3-weighted EXAFS modulations ($\Delta k = 40$–150 nm^{-1}) of the Mo K-edge and the best curve-fittings. (a) CVD-MoO_3/HSi-FAU and (b) CVD-MoO_3/NaY.

The structure of the Mo oxide species encaged in zeolite is discussed on the basis of the XAFS results. It is concluded from the XANES derivative spectra in Fig. 13 that the Mo oxide species encaged in the zeolite pores are not composed of a simple mixture of tetrahedral Mo oxide species (as observed in imp-MoO_3/NaY) and MoO_3 clusters. With CVD-MoO_3/NaY (10), the structural parameters indicate the formation of Mo oxide dimer species (Mo–Mo CN: 0.8). In conformity with this, careful sulfidation of CVD-MoO_3/NaY produced Mo sulfide dimer species encaged in NaY.[14] The formation of intrazeolite W oxide dimer species in a tetrahedral coordination was reported by Ozin *et al.*,[23,24,56–59] when $W(CO)_6$/NaY was photooxidized. According to Ozin *et al.*,[24,25] however, monomeric Mo oxide species in an octahedral symmetry were synthesized by photooxidation (80 kPa of O_2, 450 W, high pressure Xe arc lamp) of $Mo(CO)_6$/NaY in contrast to the dimer species formed by thermal oxidation at 353 K (present work) or by photooxidation[26] (20 kPa of O_2, 75 W, high pressure Hg lamp). It is conjectured that the differences in the structure of the Mo oxide species reside in the difference in the severity of the oxidation conditions of $Mo(CO)_6$: the oxidation of $Mo(CO)_6$ was completed within 1 h in the case of Ozin *et al.*[24,25] in contrast to about 16 h in the present thermal oxidation and 50 h in the previous photooxidation.[26] Obviously, it is considered that oxidation of $Mo(CO)_6$ under mild conditions is favorable for the formation of the Mo oxide dimer clusters.

The XANES spectrum for CVD-MoO_3/NaY (10) clearly indicates that the Mo atoms are in a distorted octahedral symmetry. The sum of the coordination numbers of the Mo–O bonds at 0.172 and 0.193 nm is 5.2, being consistent with the octahedral symmetry of Mo. Taking into account the coordination numbers of Mo–O and Mo–Mo (XAFS), the presence of Mo=O and Mo–O–Mo bonds (LRS and XAFS) and the chemical state of Mo(VI) (XPS), it is rational to propose that Mo_2O_6 clusters (Mo(VI) oxide dimer) are formed, interacting with the zeolite lattice oxygens to form a molecular structure as illustrated in Fig. 14. A similar dimer unit of edge-shared distorted MoO_6 octahedra is found in some Mo oxide compounds;[39] *e.g.*, in $(NH_4)_2Mo_2O_7$,[60] where R(Mo–Mo) =

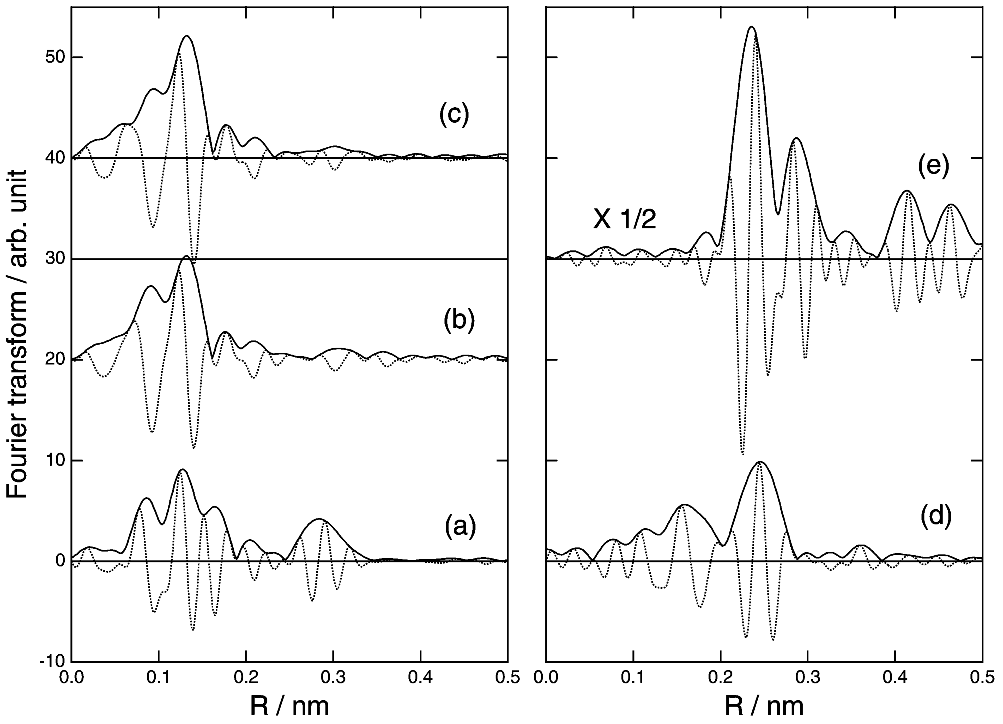

Fig. 11 Fourier transforms of k^3-weighted EXAFS modulations ($\Delta k = 40\text{–}150\ \text{nm}^{-1}$) of the Mo K-edge for (a) CVD-MoO_3/NaY, (b) CVD-MoO_3/NaY (ev), (c) CVD-MoO_3/NaY treated at 673 K for 1 h with 13 kPa of O_2, (d) CVD-MoO_3/NaY H_2-treated at 873 K for 2 h and (e) Mo metal (reference).

0.3146 nm, $R(\text{Mo=O}) = 0.1734$ and 0.1722 nm, $R(\text{Mo–O}) = 0.2069$, 0.2311, 0.2166 and 0.1840 nm. The structural parameters of the Mo oxide dimer species are in conformity with these values. Table 2 shows that CVD-MoO_3/NaY (5) has essentially identical structural parameters with CVD-MoO_3/NaY (10). It is concluded that the Mo dimer clusters are formed, irrespective of the Mo content, corresponding to 2 Mo atoms per supercage, in agreement with the observations for W oxide[56–59] and Mo sulfide[14,15] clusters encaged in zeolite. Iwasawa *et al.*[33–35] prepared a Mo oxide dimer species attached to SiO_2 by using $Mo_2(C_3H_5)_4$. The Mo atoms in the dimer are in tetrahedral symmetry in contrast to the present octahedral configuration.

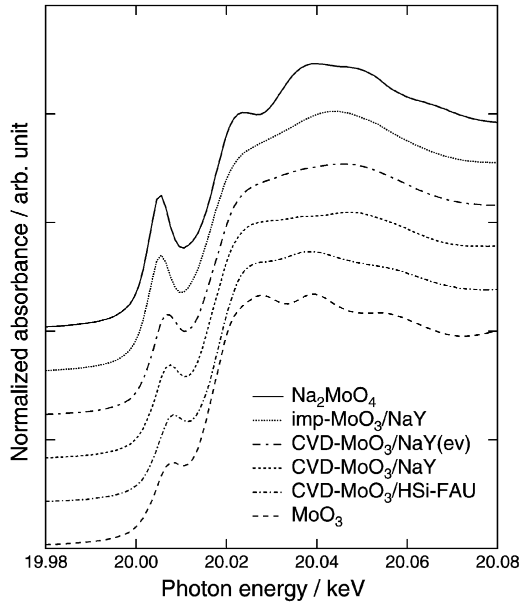

Fig. 12 XANES spectra of the Mo K-edge for the Mo oxide catalysts and reference compounds.

When CVD-MoO_3/NaY is evacuated at 673 K, the Fourier transform is considerably changed and the peak due to the Mo–Mo second shell almost disappears. However, major Mo species are still in a Mo(VI) state, although some portion of Mo is reduced to lower valence species as evidenced by a less-resolved Mo 3d band (Fig. 3(c)) and a color change from white to brown. These findings suggest a transformation of the dimer structure to a monomeric Mo(VI) species or to dimer structures so greatly distorted as to have a broad distribution of the Mo–Mo atomic distance. Taking into consideration the uniformity of the zeolite structure, however, it is most likely that the dimer oxide clusters are transformed to monomeric oxide species. The XANES spectrum of CVD-MoO_3/NaY (ev) indicates that the Mo species are in a considerably distorted octahedral symmetry. When CVD-MoO_3/NaY is treated at 673 K in the presence of gaseous O_2, a similar degradation of the dimer species to monomeric one is observed without a color change. A plausible structure is proposed in Fig. 14. The structure is similar to that proposed by Ozin *et al.*[24,25] for freshly prepared intrazeolite Mo oxide species. These findings indicate relatively low thermal stability of the intrazeolite Mo oxide dimer species.

It is considered from the structural parameters in Table 2 that the Mo oxide clusters in CVD-MoO_3/HSi-FAU consist of several Mo atoms. A possible structure is a dimer of the Mo oxide dimers, taking into account the two kinds of Mo–Mo contributions with coordination numbers of one and two. The Mo atoms are in slightly distorted octahedral symmetries. Ozin *et al.*,[57,59] proposed a similar structure for intrazeolite W oxide clusters prepared by photooxidation of $W(CO)_6$ encaged in NaY (4 W/supercage).

Larger Mo oxide clusters are formed in CVD-MoO_3/HSi-FAU than in CVD-MoO_3/NaY. A similar trend has been observed for the preparation of intrazeolite Mo sulfide clusters by using $Mo(CO)_6$ as a precursor, that is, the Mo sulfide clusters in a USY zeolite (Si/Al = 3.9) are larger in size than Mo

Table 3 The position and relative intensity of the 1s → 4d pre-edge peak and the edge energy of Mo K-edge absorption

Catalyst/reference compound	Relative intensity	Peak position[a]/eV	Edge energy[a]/eV
Na_2MoO_4	1.00	20 005.4	20 003.1
Imp-MoO_3/NaY	0.88	20 005.5	20 003.1
CVD-MoO_3/NaY (eV)	0.77	20 007.1	20 004.1
CVD-MoO_3/NaY	0.71	20 007.6	20 004.6
CVD-MoO_3/HIS-FAU	0.66	20 009.0	20 005.2
MoO_3	0.61	20 008.3	20 004.6

[a] The accuracy of the peak position and edge energy is ±0.5 eV.

sulfide dimer clusters in NaY (2.1).[15] It is considered that the cluster size of the intrazeolite Mo oxides or sulfides is correlated to the interaction strength of intermediate Mo subcarbonyl species with the host zeolite. The basic strength of the framework oxygens of the host zeolite decreases as the Si/Al ratio increases.[61,62] Since the framework oxygens coordinate to the Mo subcarbonyl species as solid ligands to form $Mo(CO)_{6-x}(Oz)_x$ (Oz: framework oxygen),[51–53,63] the decrease in the basic strength results in weaker interactions between the Mo subcarbonyl species and the framework oxygens and accordingly leads to their higher mobility during the reactions with O_2 or H_2S, accompanying the growth in the cluster size. It is also probable that the resultant Mo oxide or sulfide clusters interact less strongly with less basic framework oxygens (weaker anchoring effect), leading to a larger tendency toward agglomeration.

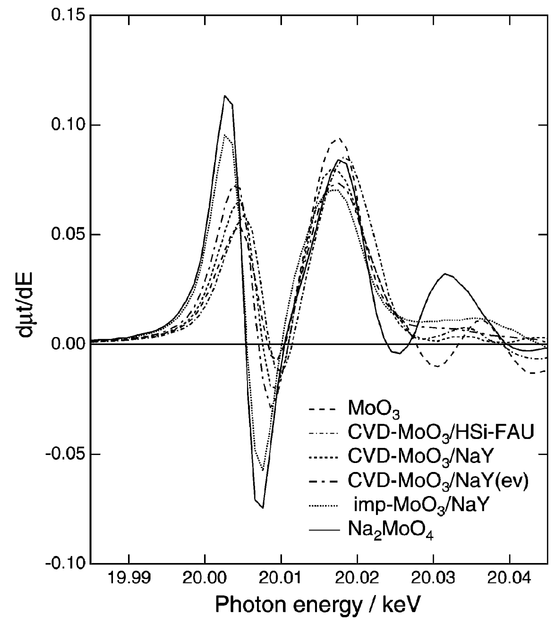

Fig. 13 The first derivatives of the XANES spectra in Fig. 12.

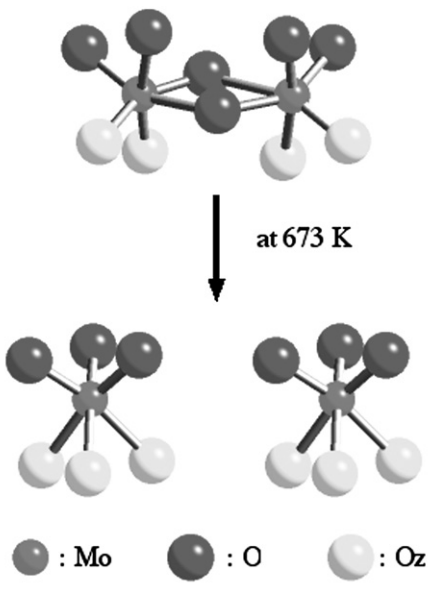

Fig. 14 Structures of the Mo oxide dimer species and monomeric species formed in CVD-MoO_3/NaY and CVD-MoO_3/NaY (ev), respectively. Oz represents the framework oxygen of the host zeolite.

In contrast to the intrazeolite Mo oxide clusters prepared from $Mo(CO)_6$, it is concluded from the EXAFS and XANES analyses that monomeric Mo oxide species in a tetrahedral symmetry are formed in imp-MoO_3/NaY, accompanying a partial degradation of the zeolite crystallinity. The formation of the tetrahedral species is also substantiated by the LRS results (Fig. 4(c)). It is proposed that MoO_4^{2-} species are combined with extra-framework Na(I) or Al(III) cations and/or Al oxides.

Structure and activity relationship

As summarized in Table 1, the specific activity of Mo oxide clusters for the oxidative dehydrogenation of ethyl alcohol decreases in the order: CVD-MoO_3/HSi-FAU ≫ CVD-MoO_3/NaY > CVD-MoO_3/NaY (ev) ≫ imp-MoO_3/NaY. As can be deduced from Fig. 2, the formation of acetaldehyde is catalyzed by the Mo oxide species and not by the host zeolite. It is considered that the activity sequence is correlated to the size and local structure of the clusters and their interactions with the zeolite. The tetrahedral Mo oxide species in imp-MoO_3/NaY strongly interact with the zeolite and are chemically robust, as observed for the Mo oxide species in MoO_3/Al_2O_3 having a low Mo content.[64,65] Okamoto *et al.*[14,15] and Vorbeck *et al.*[18] showed that the Mo oxide species in imp-MoO_3/NaY show high resistance against reduction and sulfidation at 673 K. Since SiO_2-attached monomeric Mo oxide species with a tetrahedral configuration show a comparable specific activity for the oxidation of ethyl alcohol with the Mo oxide dimer species attached to SiO_2,[34] it is considered that the low activity of imp-MoO_3/NaY results from the strong interaction with the host zeolite rather than from its tetrahedral structure of the Mo species.

The Mo oxide dimer species in CVD-MoO_3/NaY exhibit a higher specific activity than the monomeric species in CVD-MoO_3/NaY (ev). According to Iwasawa and Tanaka,[34] SiO_2-attached Mo oxide dimer species prepared using $Mo_2(\eta^3\text{-}C_3H_5)_4$ as a precursor showed a specific activity similar to Mo monomer species for ethyl alcohol oxidation at 420 K. It was shown,[34] however, that the former species show an activity per site 1.5 times higher than the latter species. Accordingly, the high specific activity and, in particular, considerably high activity per site (*ca.* 3 times higher activity per site than the monomeric species) of the present intrazeolite dimer species are ascribed to cooperative catalysis of the two Mo atoms as proposed by Iwasawa *et al.*[34] In the intrazeolite Mo oxide dimer species, two Mo atoms are strongly bonded to each other through the Mo–O–Mo bonds, while the two Mo atoms in the SiO_2-attached dimer species[33–35] are only weakly interacting, on the basis of the EXAFS results showing no Mo–Mo contributions at 200–300 K. The difference in the structures of these dimer species leads to the different catalytic activities relative to the corresponding monomeric species. It is noteworthy that CVD-MoO_3/HSi-FAU shows a specific activity 16 times higher than CVD-MoO_3/NaY. The significantly high activity of CVD-MoO_3/HSi-FAU may be due to the increased size of the Mo oxide clusters. It is considered that in the larger clusters, more effective cooperation between the Mo atoms takes place in a redox mechanism.

As shown in Fig. 2, the oxidation activity of CVD-MoO_3/NaY increases proportionally as the amount of Mo increases to 2 Mo atoms per supercage. This finding evidently demonstrates that the identical Mo oxide dimer clusters are formed irrespective of the average number of Mo atoms in the pores up to 2 Mo atoms per supercage, in conformity with the EXAFS analysis. The activity, however, significantly increases on further addition of Mo to CVD-MoO_3/NaY (10). This may be a consequence of the formation of Mo oxide clusters larger than the dimer species, although a possible activity increase due to agglomeration of the added Mo oxide species on the external surface of the zeolite cannot be ruled out. In contrast to the oxidation reaction, the formation of diethyl ether increases linearly as the Mo content increases to more than 2 Mo/supercage. This may suggest that different active sites are involved in the oxidative dehydrogenation and dehydration of ethyl alcohol. It is considered that acidic sites are generated on or near the Mo oxide species and that the acidity is less affected by the structure of the Mo oxide clusters than the oxidation activity. In line with this, the ether formation in Table 1 does not depend so much on the preparation as the acetaldehyde formation.

Conclusions

The salient findings in the present study are:

1. Intrazeolite Mo(VI) oxide dimer clusters in a distorted octahedral configuration are synthesized at 353 K by thermal oxidation of $Mo(CO)_6$ encaged in an NaY zeolite. The Mo oxide dimers are transformed to monomeric, octahedral Mo oxide species at 673 K.

2. The thermal oxidation of $Mo(CO)_6$ encaged in HSi-FAU ($Si/Al = 630$) leads to the formation of intrazeolite Mo oxide clusters containing several Mo atoms in octahedral coordinations.

3. Monomeric Mo oxide species in a tetrahedral symmetry are predominantly formed by the impregnation method.

4. The structure and size of the intrazeolite Mo oxide clusters are controlled by the zeolite composition and the heat treatment after preparation.

5. The specific activity of the Mo oxide species for the oxidation of ethyl alcohol depends strongly on the cluster size and interaction strength with the host zeolite. The activity decreases in the order: CVD-MoO_3/HSi-FAU $\gg$ CVD-MoO_3/NaY $>$ CVD-MoO_3/NaY (ev) $\gg$ imp-MoO_3/NaY.

Acknowledgement

This work was supported by CREST, Japan Science and Technology Corporation. This work was also supported by a Grant-in-Aid for Science Research from the Ministry of Education, Science, Sports and Culture (09650860). We are grateful to Mr. T. Kawabata (Shimane University) for the measurements of the XRD patterns.

References

1 G. D. Stucky and J. E. MacDougall, *Science*, 1990, **247**, 669.
2 G. A. Ozin, *Adv. Mater.*, 1992, **4**, 612.
3 G. A. Ozin, A. Kuperman and A. Stein, *Angew. Chem., Int. Ed. Engl.*, 1989, **28**, 358.
4 W. M .H. Sachtler and Z. Zhang, *Adv. Catal.*, 1993, **39**, 129.
5 B. C. Gates, *Chem. Rev.*, 1995, **95**, 511.
6 B. C. Gates, J. R. Katzer, G. C. A. Schuit, *Chemistry of Catalytic Processes*, MacGraw-Hill, New York, 1979, ch. 4.
7 (*a*) Y. Iwasawa, *Stud. Surf. Sci. Catal.*, 1996, **101**, 21; (*b*) Y. Iwasawa, *Adv. Catal.*, 1987, **35**, 187; (*c*) Y. Iwasawa, *Catal. Today*, 1993, **18**, 21.
8 J. C. Volta, J. M. Tatibouet, C. Phichitkul, J. E. Germain, *Proceedings of the 8th International Congress on Catalysis*, Dechema, Frankfurt, 1984, p. IV-451.
9 J. C. Volta and B. Morawek, *J. Chem. Soc., Chem. Commun.*, 1980, 338.
10 R. F. Howe, in *Tailored Metal Catalysts*, ed. Y. Iwasawa, Reidel, Dortrecht, 1986, p. 1141.
11 Y. Okamoto, *Catal. Today*, 1997, **39**, 45.
12 Y. Okamoto, A. Maezawa, H. Kane, T. Imanaka, in *Proceedings of the 9th International Congress on Catalysis*, ed. M. J. Phillis and M. Ternan, The Chemical Institute of Canada, Ottawa, 1988, vol. 1, p. 11.
13 Y. Okamoto, A. Maezawa, H. Kane and T. Imanaka, *J. Mol. Catal.*, 1989, **52**, 337.
14 Y. Okamoto and H. Katsuyama, *Ind. Eng. Chem. Res.*, 1996, **35**, 1834.
15 Y. Okamoto, H. Katsuyama, K. Yoshida, N. Nakai, M. Matsumoto, Y. Sakamoto, J. Yu and O. Terasaki, *J. Chem. Soc., Faraday Trans.*, 1996, **92**, 4647.
16 Y. Okamoto, H. Okamoto, T. Kubota, H. Kobayashi and O. Terasaki, *J. Phys. Chem. B*, 1999, **103**, 7160.
17 Y. Okamoto and T. Kubota, *Catal. Surveys from Japan*, 2001, **5**, 3.
18 G. Vorbeck, W. J. J. Welters, L. J. M. van de Ven, H. W. Zanbergen, J. W. de Haan, V. H. J. de Beer and R. A. van Santen, *Zeolites and Related Microporous Materials: State of the Art*, Elsevier, Amsterdam, 1994, p. 1617.
19 W. J. J. Welters, PhD Thesis, Eindhoven University of Technology, The Netherlands, 1994.
20 P. de Pont, PhD Thesis, Delft University of Technology, The Netherlands, 1998.
21 M. J. Vissenberg, PhD Thesis, Eindhoven University of Technology, The Netherlands, 1999.
22 M. Laniecki and W. Zmierczak, *Zeolites*, 1991, **11**, 18.
23 G. A. Ozin and S. Özkar, *Chem. Mater.*, 1992, **4**, 511.
24 G. A. Ozin, S. Özkar and R. A. Prokopowicz, *Acc. Chem. Res.*, 1992, **25**, 553.
25 R. Jelinek, S. Özkar and G. A. Ozin, *J. Phys. Chem.*, 1992, **96**, 5949.
26 Y. Okamoto, Y. Kobayashi and T. Imanaka, *Catal. Lett.*, 1993, **20**, 49.
27 K. Asakura, Y. Noguchi and Y. Iwasawa, *J. Phys. Chem. B*, 1999, **103**, 1051.
28 T. Komatsu, S. Namba, T. Yashima, K. Domen and T. Onishi, *J. Mol. Catal.*, 1985, **33**, 345.
29 M. Niwa, M. Mizukami, M. Takahashi and Y. Murakami, *J. Catal.*, 1981, **70**, 14.
30 J. Tatibouet, J. M. Germain and J. C. Volta, *J. Catal.*, 1983, **82**, 240.
31 J. C. Chung, R. Miranda and C. O. Bennett, *J. Catal.*, 1988, **114**, 398.
32 C. Louis, J. M. Tatibouet and M. Che, *J. Catal.*, 1988, **109**, 354.
33 Y. Iwasawa and M. Yamagishi, *J. Catal.*, 1983, **82**, 373.
34 Y. Iwasawa and H. Tanaka, in *Proceeding of the 8th International Congress on Catalysis*, Dechema, Frankfurt, 1984, p. IV-381.
35 Y. Iwasawa, *Tailored Metal Catalysts*, ed. Y. Iwasawa, Reidel, Dortrecht, 1986, p.1.
36 M. Niwa, H. Yamada and Y. Murakami, *J. Catal.*, 1992, **134**, 331.
37 T. J. Yang and J. H. Lunsford, *J. Catal.*, 1987, **103**, 55.
38 K. Tanabe, *Solid Acids and Bases*, Kodansha, Tokyo, 1970.
39 (*a*) F. A. Cotton, G. Wilkinson, *Advanced Inorganic Chemistry*, Wiley, New York, 1988, pp. 807–819; (*b*) N. N. Greenwood and

A. Earnshaw, *Chemistry of the Elements*, Pergamon, Oxford, 1984, ch. 23.

40 (*a*) R. B. Quincy, M. Houalla, A. Proctor and D. M. Hercules, *J. Phys. Chem.*, 1990, **94**, 1520; (*b*) M. Yamada, J. Yasumaru, M. Houalla and D. M. Hercules, *J. Phys. Chem.*, 1991, **95**, 7037.

41 F. D. Hardcastle and I. E. Wachs, *J. Raman Spectrosc.*, 1990, **21**, 683.

42 W. P. Griffith and P. J. B. Lesniak, *J. Chem. Soc. A*, 1969, 1066.

43 H. Knözinger and H. Jeziorowski, *J. Phys. Chem.*, 1978, **82**, 2002.

44 R. Cid, F. J. Gil Lalambias, J. L. G. Fierro, A. Lopez Agudo and J. Villasenor, *J. Catal.*, 1984, **89**, 478.

45 R. Cid, F. Ovellana and A. Lopez Agudo, *Appl. Catal.*, 1987, **32**, 327.

46 J. L. G. Fierro, J. C. Conesa and A. Lopez Agudo, *J. Catal.*, 1987, **108**, 334.

47 J. Thoret, C. Marchal, C. Doremieux-Morin, P. P. Man, M. Gruia and J. Fraissard, *Zeolites*, 1993, **13**, 269.

48 (*a*) J. C. J. Bart, *Adv. Catal.*, 1986, **34**, 203; (*b*) S. Yoshida and T. Tanaka, in *X-Ray Absorption Fine Structure for Catalysts and Surfaces*, ed. Y. Iwasawa, World Scientific, Singapore, 1996, p. 304.

49 P. Gallezot, G. Coudurier, M. Primet and B. Imelik, *ACS Symp. Ser.*, 1977, **40**, 144.

50 Y. Yong-Sing and R. F. Howe, *J. Chem. Soc., Faraday Trans. 1*, 1986, **82**, 2887.

51 Y. Okamoto, A. Maezawa, H. Kane, I. Mitsushima and T. Imanaka, *J. Chem. Soc., Faraday Trans. 1*, 1988, **84**, 851.

52 S. Özkar, G. A. Ozin, K. Moller and T. Bein, *J. Am. Chem. Soc.*, 1990, **112**, 9575.

53 Y. Okamoto and T. Kubota, *Microporous Mesoporous Mater.*, 2001, **48**, 301.

54 M. J. Almond, J. A. Crayston, A. J. Downs, M. Poliakoff and J. J. Turner, *Inorg. Chem.*, 1986, **25**, 19.

55 M. J. Almond and J. Downs, *J. Chem. Soc., Dalton Trans.*, 1988, 809.

56 G. A. Ozin, S. Özkar and P. Macdonald, *J. Phys. Chem.*, 1990, **94**, 6939.

57 G. A. Ozin and S. Özkar, *J. Phys. Chem.*, 1990, **94**, 7556.

58 K. Moller, T. Bein, S. Özkar and G. A. Ozin, *J. Phys. Chem.*, 1991, **95**, 5276.

59 G. A. Ozin, R. A. Prokopowicz and S. Özkar, *J. Am. Chem. Soc.*, 1992, **114**, 8953.

60 A. W. Armour, M. G. B. Drew and P. C. H. Mitchell, *J. Chem. Soc., Dalton Trans.*, 1975, 1493.

61 W. J. Mortier and R. A. Schooheydt, *Prog. Solid State Chem.*, 1985, **16**, 1.

62 Y. Okamoto, *Crit. Rev. Surf. Chem.*, 1995, **5**, 249.

63 Y. Okamoto, T. Imanaka, K. Asakura and Y. Iwasawa, *J. Phys. Chem.*, 1991, **95**, 3700.

64 C. P. Li and D. M. Hercules, *J. Phys. Chem.*, 1984, **88**, 456.

65 H. Knözinger, *Proceedings of the 9th International Congress on Catalysis*, ed. M. J. Phillips and M. Ternan, The Chemical Institute of Canada, Ottawa, 1988, vol. 5, p. 20.